Differential Spectral Extraction for JWST's NIRISS-SOSS Instrument

William Frost[a], **Loïc Albert (PhD)**[b], **and René Doyon (PhD)**[b]

[a]Department of Physics, McGill University, 3600 Rue Université, Montréal, QC, H3A 2T8, Canada
[b]Department de Physique, Université de Montréal, 1375 Avenue Thérèse-Lavoie-Roux, Montréal, QC H2V 0B3

This manuscript was compiled on January 1, 2021

Among the James Webb Space Telescope (JWST) instrument suite, the Near InfraRed Imager and Slitless Spectrograph (NIRISS) will allow for spectroscopy and imaging in the near-IR range. With one of the JWST's goals being precise exoplanet characterization, NIRISS is equipped with a Single-Object Slitless Spectroscopy (SOSS) mode designed for transit spectroscopy. Alongside its advantages, the slitless nature of NIRISS-SOSS carries with it certain drawbacks in the form of spectral contamination. In particular, spectral features from unwanted objects in the NIRISS field can overlap with those of a target star, which can hide planetary atmospheric signals of interest. This work implements a technique to remove the field contamination present in NIRISS-SOSS data. The technique, referred to as a differential spectral extraction, assumes that out-of-transit exposures have a constant spectrum. By subtracting the mean of those exposures from all exposures in a time series, a residual spectrum is obtained with absorption features due only to a transiting exoplanet. Adding back the target star's spectrum (obtained through models or other observations) to the time series outputs an uncontaminated version of what was initially observed. This work shows that differential spectral extraction is successful in decontaminating simulated NIRISS-SOSS time series, where the stellar systems studied had smooth black-body behaviour and planet models showed no atmospheric features (i.e. R_p/R_* is constant). We also quantify the error this technique can introduce based on the inaccuracy of the surface temperature value for the injected stellar model. Results show that for the recovered transit depths to remain within errors of $\sim$30 ppm, the injected stellar model's surface temperature should be accurate to within $\pm$10 Kelvin.

Exoplanet | Transit | Spectroscopy | JWST | NIRISS

1. Scientific Context

Since it's first breakthroughs in the mid 90's, the importance that exoplanet research has in modern astrophysics has evolved quite dramatically. From initial observations in the 1990s all the way into the 2000s, the rate of discovery kept increasing, albeit at a slow rate. During the 2010s, instruments like the Kepler and TESS telescopes increased that rate dramatically, leading to the confirmation of several thousands of alien worlds[1]. The paradigm-shift in the exoplanet research community and the amount of knowledge brought upon by these results are a testament to the technology and the people involved.

Nevertheless, much is still to be discovered in this field. For example, the most effective technique for exoplanet discovery combines the transit and radial velocity methods to output characteristics like planet size, mass, density and orbital parameters. Although this information is invaluable, with density being a key factor in differentiating terrestrial and gas planets, it does not allow for in-depth characterization. Whether one's motivation is the search for life or to further document exoplanet diversity, more information is needed.

Therefore, one of the next frontiers for exoplanet research lies in characterizing their atmospheres. An option for pursuing this is through transmission/transit spectroscopy. The aim of this technique is to obtain the spectrum of a known host star during a planetary transit. By looking at how the spectrum with respect to wavelength dips during transit, we can infer information about the planet's perceived size over those wavelengths. An increased size compared to its base value means more starlight is being blocked by molecules capable of absorbing light at that wavelength. Thus, it is possible to characterize an exoplanet atmosphere's molecular composition and the abundance of those molecules using transit spectroscopy.

Currently, both ground-based (e.g. HARPS[2], FORS2[3]) and space-based (e.g. Hubble[4], Spitzer[5]) telescopes have been able to perform transmission spectroscopy measurements of various planet types. Although most of the currently available data is for large planets relative to their star ($\frac{R_p}{R_*} \approx 0.1$), some of it characterizes planets as small as super-Earths having $\frac{R_p}{R_*} \approx 0.02$ [1]. Because larger planets block more light, the fraction of the blocked light due to atmospheric features is more easily discerned. However, potential Earth-like planets around Sun-like stars have $\frac{R_p}{R_*} \approx 0.01$. The small fractions of light that these planet's atmospheres absorb make it difficult or impossible for current instrumentation to confidently detect

Significance Statement

One of the functions of the James Webb Space Telescope will be to study transiting exoplanets and their atmospheres. Due to the JWST's precise observation capabilities, it will allow the previously undetectable atmospheric features of low-volume planets to be resolved. To accomplish this, one the instruments it will use is the Near InfraRed Imager and Slitless Spectrograph (NIRISS) in its Single-Object Slitless Spectroscopy (SOSS) mode. The slitless nature of NIRISS-SOSS means that NIRISS field-of-view objects are more likely to have their spectra overlap with the spectral orders of a target star. Since this field contamination could hide small atmospheric signals of interest, it preferably has to be accounted for. At the moment, the only implemented solution is to observe during times with low field contamination. By removing field contamination from a NIRISS-SOSS observation run, it would allow JWST users to observe a greater variety of exoplanet systems and reduce the complexity of scheduling observations

[1]To whom correspondence should be addressed. E-mail: william.frost2mail.mcgill.ca

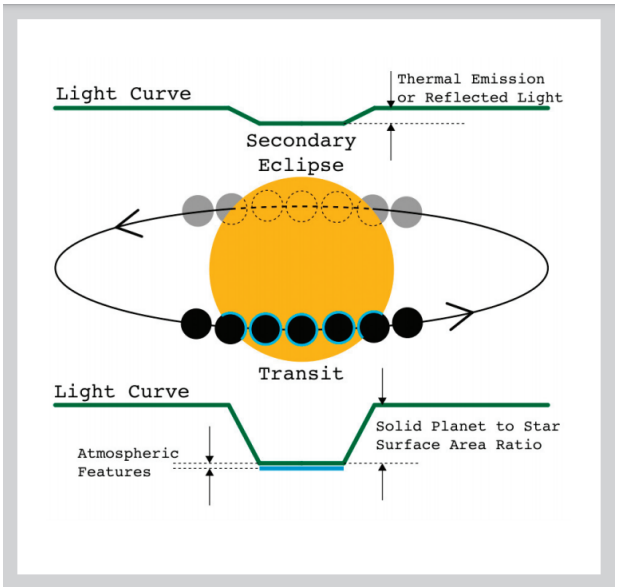

Fig. 1. (Taken from (6)) It shows the the 2 types of light curves that occur when observing a planetary system along its orbital plane. Here, the star is the yellow circle, while the planet is represented by a black or grey circle depending on if its in front or behind its host star relative to an observer. The planet's atmosphere is shown in light blue. With transit spectroscopy, we look for slight variations in a star's transit light curve due to a planetary atmosphere absorbing light at certain wavelengths.

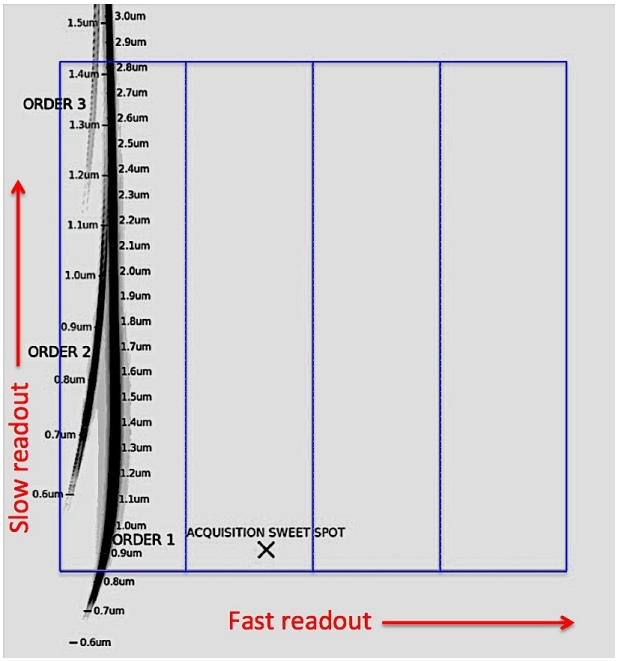

Fig. 2. (Taken from (7)) Layout of GR700XD spectra on the NIRISS detector. NIRISS uses a 2048x2048 detector grid, illustrated by the outer blue square perimeter. In this image, the vertical axis corresponds to the spectral axis, while the horizontal is defined as the spatial axis. The standard readout mode uses spectral pixels [0,2048] and spatial pixels [0,256] (origin here is in the upper left-hand corner). This standard readout includes spectral orders 1,2 and 3 of a target star. Other readout modes include a full-detector and bright-mode read-out, where the latter only includes the first order. The acquisition sweet spot defines where the target star must show up on the detector in order for its spectrum to be properly spread out among the readout pixels.

them. In addition, many observations of planets with known transmission spectroscopy can benefit from more precise data.

JWST and NIRISS

Enter the James Webb Space Telescope (JWST), scheduled to launch in the fall of 2021. With its mirror capable of collecting 6 times more light than the Hubble Space Telescope and equipped with a diverse instrument suite, the JWST is poised to make important contributions to exoplanet science. The distinct advantage Webb has over any advanced ground facility is the complete lack of atmospheric noise with its observations. These conditions lead to increased signal-to-noise ratios (SNR) and make exoplanet atmospheric signals easier to detect when performing transit spectroscopy. With a plethora of known TESS, Kepler and other planets to observe, there is no shortage of candidates for atmospheric characterization using JWST.

The scientific instrument this paper is concerned with, the Near InfraRed Imager and Slitless Spectrograph (NIRISS), is provided by the Canadian Space Agency and one of the four aboard Webb. It is designed for slitless spectroscopy, imaging and high-contrast interferometric imaging between wavelengths of 0.6-5.0 μm over a 2.2' x 2.2' field of view. For time series observations of planetary transits, NIRISS has a Single-Object Slitless Specroscopy (SOSS) mode optimized for such events. With a resolution of $R \equiv \frac{\lambda}{\delta\lambda} \simeq 700$, the SOSS mode observes between 0.6-2.8 μm using 3 cross-dispersed spectral orders [7]. Some notable molecular absorption features within this range include H_2O, O_2, CO_2 and CH_4 [8][6], which are key molecules to assess the habitability of terrestrial exoplanets.

NIRISS-SOSS is designed to observe stars with J-band Vega magnitudes between 7 and 15. In addition, due to the minute changes in spectra that needed to be observed, the instrument's stability is paramount. To achieve the required stability, the GR700XD grism NIRISS-SOSS uses for spectroscopy has a cylindrical lens that defocuses the spectral orders in the spatial direction. This spreads the incoming starlight onto a larger subset of the detector which helps mitigate the effects of flat field errors and pointing jitter. It also allows for brighter objects to be observed without saturating the detector[7]. Fig-2 demonstrates the layout of spectra as seen by NIRISS-SOSS.

NIRISS-SOSS Spectral Contamination

Along with its advantages, the SOSS design carries with it certain drawbacks in the form of spectral contamination. Here, contamination refers to spectral traces intersecting with each other on the detector. With NIRISS-SOSS, this phenomena manifests as either overlap or field contamination.

Overlap Contamination.

This is intrinsic to the instrument itself. It comes from the order 2 trace of the target star overlapping with it's brighter order 1 trace at longer wavelengths. Fig-2 shows this overlap in effect in the upper left-hand corner of the figure. This problem affects the extraction of the order 2 trace the most, as its throughput on this part of the detector is an order of magnitude smaller than the order 1 throughput.

A technique is currently being developed by Ph.D student Antoine Darveau-Bernier (Université de Montréal) and others to help deal with this overlap contamination. Currently, an official paper on this technique cannot be referenced. However,

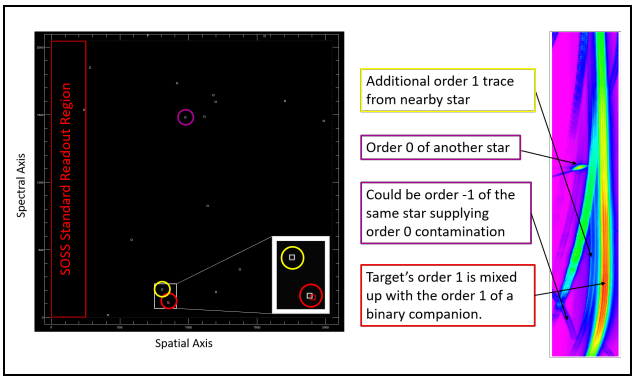

Fig. 3. Simulated NIRISS field-of-view (FOV) (left) and SOSS exposure (right) of the binary star system LHS-6343. The desired target is shown as a hollow red square centered on the NIRISS acquisition sweet spot. Hollow white squares represent other stars in the FOV. The exposure on the right presents many undesired spectral lines that can be retraced to certain sources in the FOV. Colored circles in the FOV match with colored outlines of text which point out the contributions of that color to the SOSS field contamination. In this case, the binary companion of the target star remains in the FOV regardless of observation scheduling and permanently overlaps with our target spectrum. Thus, field contamination is unavoidable when observing binary systems with NIRISS-SOSS.

for this work, we assume that this form of contamination is non-existent in the simulated data used. This assumption is upheld by simulating NIRISS-SOSS spectral orders on separate detector grids, and is necessary to quantify the errors produced by the differential extraction method; the main topic of this work which addresses the second form of contamination.

Field Contamination.

One of the perks of using slits in spectroscopy is the increased control of which light sources contribute to the spectrum. With NIRISS slitless spectroscopy, spectra from unwanted sources in the field of view have an increased chance of getting mixed up with our target's spectrum. Fig-3 shows an example of such field contamination for a SOSS simulation of a transiting brown dwarf in the binary system LHS-6343.

It is possible to minimize this field contamination by optimally orienting the JWST's field of view. Since the acquisition sweet spot (see Fig-2) is close to the perimeter of the detector, mirror rotations where the target remains centered on the sweet spot will change the portion of space that NIRISS sees; and may lead to less field contamination for a given target.

However, the range of acceptable position angles is dependent on the JWST's orbit around the Sun, since the instrument needs to continually maintain its sun shield facing towards it. Therefore, minimizing field contamination requires carefully selecting observation dates such that the previous constraint is met. To assist with optimal scheduling, a tool[9] has been developed by the NIRISS-SOSS team.

Scheduling may be sufficient for some observations, but no such mitigation strategy works for exoplanets in crowded fields. This is particularly problematic for terrestrial exoplanets with tiny spectroscopic signals that can easily be hidden by field contaminants. In addition, this potential scheduling constraint coupled with limited telescope time and fierce competition for JWST use could render some projects infeasible. The main goal of this work now comes into focus: implement a technique to remove the field contamination likely present in NIRISS-SOSS spectra.

2. The Differential Extraction Method (DEM)

There can be many solutions to removing field contamination. One approach would be to model the spectra of relevant stars in the field, determine where their spectral traces fall on the detector and subtract them. This can be possible given a good understanding of the SOSS mode and of all stars in the field. However, the amount of additional information (especially the contaminating spectra) one has to gather for this task is a non-negligible endeavour. We instead present a simpler method which only requires knowledge of the target star's spectrum. We refer to this technique as a **differential spectral extraction**.

The main assumption here is that out-of-transit SOSS exposures have a constant spectrum. Thus, the only variations in the spectrum of a SOSS time series are caused by a transiting exoplanet. By subtracting the mean of the out-of-transit exposures from all exposures in a time series, a residual spectrum is obtained containing absorption features due only to the transiting exoplanet. Any source of constant contamination is effectively removed.

Once differential exposures are created, the flux on the detector is integrated (in the same way it would be in the non-differential case) to obtain a 1D differential spectrum of photon counts over wavelength. Given a well-known target star spectrum (e.g. from a JWST instrument, other instruments or stellar models), it can be added back to the differential spectra of the time series to obtain an uncontaminated version of what was initially observed.

Once a clean time series of spectra are obtained, light curves can be plotted for each wavelength in the spectrum. Fitting these light curves and retrieving either their transit depth ($\frac{\Delta F_*}{\Delta F_*}$) or planet radius ($\frac{R_p}{R_*}$) parameters makes it possible to produce a transit spectroscopy plot.

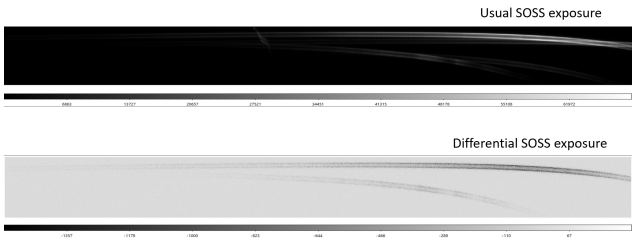

Fig. 4. Comparison of a usual and differential simulated SOSS exposure. Both the images and their scales are linear. The usual SOSS exposure shown here has various constant field contaminants overlapping with the target signal. Once the mean of the out-of-transit exposures has been subtracted from the time stream, differential exposures are obtained containing negative spectrum dips caused by planetary atmospheric signals. In essence, SOSS differential exposures are un-normalized, 2D absorption spectra of exoplanet atmospheres.

3. Simulation and Extraction Methods

SOSS Simulation Software.

The simulation tools used to generate SOSS time series are provided by Jason Rowe (Ph.D) (Bishop's University). A paper is yet to be published on the simulation software, but a prototype version was available for this work. What follows is a brief description of the process.

The main code is written in Python, while certain subroutines wrap FORTRAN code to speed up basic computations.

The simulation takes in a file of observational parameters like the integration time of an exposure and the detector readout region, as well as planetary orbit parameters. The input exoplanet atmosphere model has values of $\frac{R_p}{R_*}$ as a function of wavelength. The star's spectrum is obtained from an ATLAS-9 model with non-linear limb darkening (4 coefficients) at each wavelength. To model NIRISS-SOSS spectral traces, reference files with information about trace coordinates and detector point-spread functions[10] (PSFs) are used.

With these inputs, the simulation software iterates through time and creates a desired amount of observations. The output is a time series of 2D exposures (arrays) of the desired spectral orders, where the size of the arrays depend on the readout dimensions.

NIRISS-SOSS Spectrum Extraction.

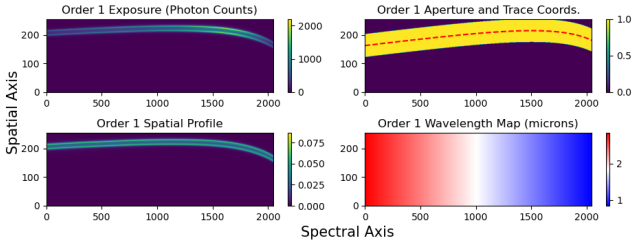

Fig. 5. Visual representations of the various reference files needed in NIRISS-SOSS spectrum extraction. **Top-left** is a simulated SOSS exposure for order 1 as seen by the detector in standard readout mode (256x2048). **Top-right** shows an aperture with width=80 pixels and the trace coordinates plotted in red. By defining such an aperture, only the pixels that fall within the yellow region will be integrated to create the spectrum for order 1. **Bottom-Left** shows the normalized spatial profile of order 1 on the detector. **Bottom-right** shows the wavelength mapping for order 1.

Once the simulations are complete, extracting a time series of spectra from SOSS exposures requires reference files with information on the spectral trace coordinates, as well as the spatial profiles and wavelength mappings of the detector pixels, for all relevant orders. For the purposes of this work, only orders 1 and 2 are considered.

The trace coordinates are used to tell the extraction process which detector pixels to integrate. By imposing a fixed-width aperture centered along the trace coordinates of a spectral order, an integration region is defined on the detector which contains photon counts from that order and from potential contaminants.

The spatial profile is used to determine the weight of an order's contribution to the flux found on any detector pixel. This information is very important when it comes to solving the overlap contamination problem mentioned earlier. For this work, since orders 1 and 2 are simulated on separate detectors, spatial profiles are not as useful. Their use can mitigate the effects of some field contaminants, but those who fully cross over the target spectrum will still have their flux contributions integrated.

The wavelength mapping ensures that the correct detector pixels are integrated for a given wavelength binning of the spectrum. This mapping is important since each spatial column of pixels perpendicular to the spectral axis cannot be assumed to harbour a unique wavelength. In fact, the true wavelength mapping of the NIRISS-SOSS detector is tilted as a function of wavelength. Although this tilt is estimated at less than 3^o with respect to the spatial axis, not taking it into account (i.e. summing columns) can lead to sharp spectral details being absent or distorted in the final transmission spectroscopy plots.

4. Differential Extraction Method Performance

The goal of this paper is to quantify the performance of the DEM and its ability to output correct spectra. To measure this performance, the results are compared to the expected transit spectroscopy for the simulated system. By doing this, we wish to know if the method introduces errors that are specific to it. We also want to get an idea for the required accuracy in target star models used in the DEM in order for results to remain close to reality. And finally, this work demonstrates the advantage of the DEM on a simulated system with constant field contamination.

Model Setup.

To limit extraction errors linked to the complexity of the data, a simple planetary system is modelled. This is done to ensure that the DEM is sound in the best case. The chosen simple system has a star with a smooth, featureless black-body spectrum; derived from a surface temperature of T=5778 Kelvin and scaled such that it does not saturate the detector. For this work, because the simulated SOSS exposures are generated without noise, the amount of counts the detector gets per integration has no effect on the results. As long as the scaled stellar model input to the simulation generated counts which did not cause numerical errors during extraction, it was deemed sufficient. In addition, the stellar model was created with no limb darkening features to simplify transit light curve fitting.

The simulation's planetary atmosphere model is a constant $\frac{R_p}{R_*} = 0.1$ over the model's wavelength range. This represents a planet with no atmosphere; and serves as an effective best case for testing the DEM. In addition, since the planet models are compared to transit depth calculations, the relationship between the planet radius ($\frac{R_p}{R_*}$) and the (normalized) transit depth

$$depth = \frac{\Delta F_*}{F_*} = \left(\frac{R_p}{R_*}\right)^2 \quad [1]$$

is used to convert between the two. Since the model stellar spectrum has no limb-darkening, Eq-1 becomes exact so long as the entire planet passes in front of its star. This is case for this work's simulations as the orbital impact parameters were set to 0, meaning the planets passed directly in the center of their host stars relative to the observer.

Another important simplification for this work is that wavelength maps were assumed to have no tilt, even though the simulation tools do produce "tilted" exposures. This effectively means that the wavelength binning for the spectra of the time series will not be correct. However, since most of the photons of a spectral order fall within ~ 30 pixels along the spatial axis, a tilt in the wavelength mapping of $\leq 3^o$ should displace wavelengths by no more than a couple of spectral pixels on average. For time series with fine spectral features, this would pose a problem. However, for this work's constant planet models and smooth stellar spectra, the effect of tilt should be less pronounced.

Finally, it is worth repeating that the simulated SOSS exposures used for this work have no overlap contamination, meaning each spectral order was produced on separate detectors. However, the simulated exposures may harbour some field contamination. This change does not impact the DEM and is done only to isolate the errors produced by it.

Quantifying The Best-Case Performance.

The best case is essentially defined as a time series with no overlap contamination and with either absent or truly constant field contamination. Since the mean of out-of-transit exposures are subtracted from the time series, whether constant field contamination was present or not has no effect on this simulation's end result. In this idealized system, only the target star spectrum that is added back has any effect. Therefore, the following transmission spectroscopy plots were derived from a best-case simulation with no field contamination and where a perfect target star spectrum is available.

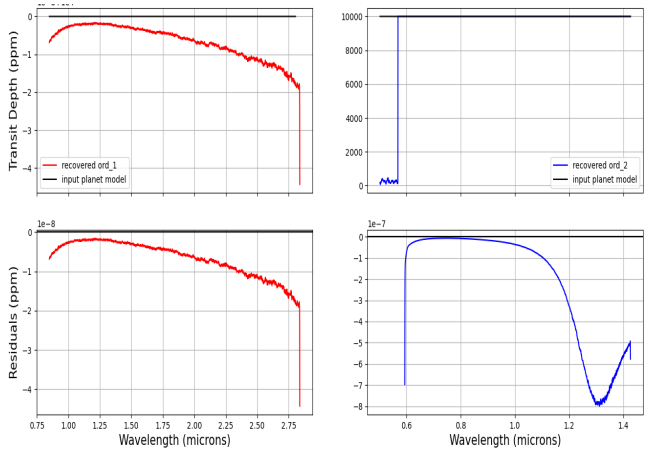

Fig. 6. Transmission Spectroscopy plots of a simulated system with a constant planet model and a black-body stellar spectrum. The results are obtained using the DEM. The red and blue curves represent order 1 and 2 realizations respectively. Black curves represent the expected transit depth given the planet model used. For both orders, residuals on the order of 10^{-8} and 10^{-7} ppm were obtained. In the top-right plot representing order 2, the sudden dip in transit depth at short wavelengths can be attributed to the order 2 trace leaving the readout region. To better see the true residuals for order 2, that plot omits those wavelengths.

Fig-6 shows that for both orders, the error in recovered transmission spectroscopy using the DEM is orders of magnitude smaller than a part-per-million (ppm). With such small deviations from the expected result, the observed discrepancies could be attributed to slight systematic errors in the spectrum extraction process. These plots show that under the assumption of constant field contamination, the only source of error in the DEM outputs is the accuracy of the injected target star spectrum.

Quantifying Errors Introduced By Injected Target Spectra.

In the best case, differential extraction is performed with perfect knowledge of the target star spectrum. These next simulations are used to observe the errors that occur when an inaccurate spectrum is supplied to the DEM.

The observed trend is that (unsurprisingly) hotter star models lead to underestimates in transit depth while cooler models have the opposite effect. The discrepancy between expected and obtained results is felt greater at short wavelengths due

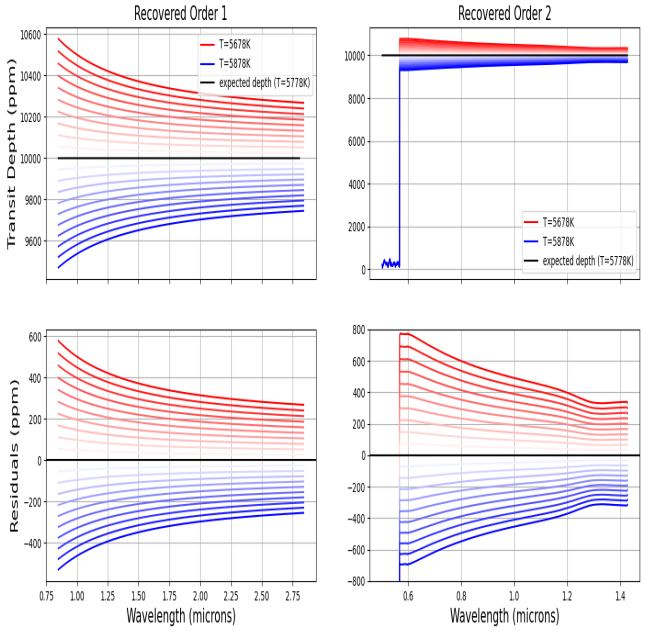

Fig. 7. Transmission Spectroscopy plots of a simulated system with a constant planet model and a black-body stellar spectrum. Results obtained using the DEM. The plots to the left represent order 1 extractions, while those to the right represent order 2. Black curves represent the expected transit depth of the simulations. Blue-shifted curves represent extractions where the target star spectrum had black-body temperatures $T_{injected} > T_{actual}$, and red-shifted curves show the effects where $T_{injected} < T_{actual}$. The explored temperature range was ± 100 K from the target's actual $T = 5778$ K, at intervals of 10 K. For order 2 realizations, the dip in transit depth at short wavelengths has the same explanation as in Fig-6. The plots show that for errors of ± 100 K in the surface temperatures for injected stellar models, deviations between 10^1 and 10^3 ppm arise from those errors.

a greater rate of change in the flux of the black-body stellar spectrum in that wavelength range.

Testing On A Simulation With Field Contamination.

The final showcase for the differential extraction method in this work is be performed on the same simple system as before, but with injected field contamination in the simulated SOSS exposures. To reproduce contamination, an analog to a binary companion star is projected onto the detector, as well as some order 0 traces. These constant contaminating spectra were generated from a stellar model with spectral features present and a temperature $T \approx 6000$ K using J. Rowe's previously mentioned simulation software.

From Fig-8, the transit spectroscopy obtained from contaminated exposures shows that without differential treatment, the planet model input to the simulation cannot be properly retrieved. Even if the exposures were to be weighted with the known spatial profiles of orders 1 and 2, the contamination remains present. This is true especially at longer wavelengths where the orders of the binary companion overlap with the target's orders on the detector.

If the DEM is used to analyse these exposures, the results would look identical to Fig-6 since the contamination introduced to the simulation was truly a constant over time. For systems with persistent field contamination like the one simulated here, differential extraction provides a simple solution for optimal spectrum retrieval.

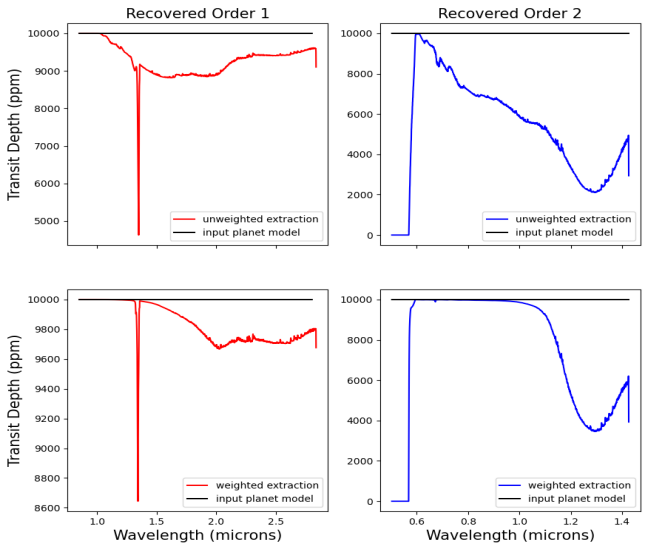

Fig. 8. Transmission Spectroscopy plots of a simulated system with a constant planet model, a black-body stellar spectrum and constant field contamination. Results obtained without the DEM (i.e. aperture integration over untouched SOSS exposures). The plots to the left represent order 1 extractions, while those to the right represent order 2. Black curves represent the expected transit depth of the simulations. The top plots are obtained without weighting the detector pixels by an order's spatial profile, while the bottom plots do. The sharp dip in order 1 curves at 1.3 microns are due to the presence of a contaminating order 0 trace. For order 2 realizations, the dip in transit depth at short wavelengths has the same explanation as in Fig-6.

5. Discussion

Although this work presents preliminary findings on the performance of the differential spectrum extraction method applied to NIRISS-SOSS, some meaningful insight is still gained from its results.

For the best-case results shown in Fig-6, we show that the planet model is recovered accurately under noiseless simulation conditions and a perfect knowledge of the target star spectrum. In real life applications, photon (Poisson) noise and instrument systematics would contribute to the error as well. In addition, if the prime assumption of the DEM (constant out-of-transit spectrum) is not valid for a given target, additional offsets can be introduced to the transit spectroscopy results. Solutions to the latter problem include modeling the incoming flux and subtracting the contributions from inconstant sources, which is a solution akin to the one mentioned in the beginning of section 2. Otherwise, simply restricting the amount of out-of-transit exposures in the time series will likely increase the validity of the prime assumption, at the expense of increasing the error brought upon by subtracting the mean of exposures during the DEM.

When observing the behaviour of the DEM as a function of the injected stellar model, we observe that misjudging the target star's temperature can induce noticeable errors ($\sim 10^2$ ppm) in the recovered transit spectroscopy curves. Even for large planets with transit depth on the order of 10^3 ppm, atmospheric signals are expected to be no more than a few percentages of their base depth values. This means looking for defined dips of a few tens of ppm will require either accurate stellar modeling or precise spectral observations. In the former case, current and future instrumentation can obtain these spectra at the cost of valued telescope time. On the other hand, this work has shown that if models are to be used for the DEM instead, they should aim at being accurate within ± 10 K of the target star's temperature, let alone accurately representing the star's own spectral features.

6. Concluding Statements

In the end, this work has shown that differential spectral extraction with NIRISS-SOSS is a viable option for correctly extracting spectra from SOSS exposures. Although the required precision of the outside information used for extraction increases as fainter atmospheric signals are observed, the DEM still offers a cost-effective way of dealing with field contamination. Due to the highly competitive nature of JWST telescope time and the faint targets that JWST exoplanet research wishes to study, the DEM has the potential to simplify the planning process for observations of crowded NIRISS fields. It can also allow for slitless spectroscopy observations that are otherwise infeasible with traditional extraction techniques.

With this work laying the foundation for the DEM and its performance, future work has the opportunity to further characterize and optimize the differential extraction process as well as apply it to increasingly complex systems. Plans include:

- Performing the DEM on simulations with actual atmospheric signals to observe. How does the accuracy of the injected target star spectrum affect the ability to extract sharp, finely resolved signals? As the complexity of stellar and planetary models increases, is it still feasible to use them in the DEM or should actual observations be used instead? Can the DEM errors remain under the photon noise limit for realistic simulations?

- Performing the DEM on observed targets in crowded fields with existing transmission spectroscopy curves. This would show that the DEM can correctly extract spectra from actual data. The proposed test would be on LHS-6343 data from Hubble's Space Telescope Imaging Spectrograph. Can the atmospheric features of the transiting brown dwarf LHS 6343c be resolved?

- Fully incorporating the extraction tools meant to deal with overlap contamination with the DEM. A combination of both extraction techniques is what will need to be done on actual data coming from the JWST.

ACKNOWLEDGMENTS. Immense thanks go out to René Doyon and Loïc Albert for supervising this research and for giving me the opportunity to work with them and their team. Thanks are also attributed to Antoine Darveau-Bernier for his help related to optimal NIRISS-SOSS extraction techniques. Additional thanks are awarded to Jason Rowe for his help in understanding the SOSS simulation software.

References

1. Nasa exoplanet archive (exoplanetarchive.ipac.caltech.edu) (2020).
2. A Wyttenbach, D Ehrenreich, C Lovis, S Udry, F Pepe, Spectrally resolved detection of sodium in the atmosphere of hd189733b with the harps spectrograph. *Astron. Astrophys.* **577**, A62 (2015).
3. J Wilson, et al., Ground-based transmission spectroscopy with fors2: A featureless optical transmission spectrum and detection of h2o for the ultra-hot jupiter wasp-103b. *Mon. Notices Royal Astron. Soc.* **497**, 5155–5170 (2020).

4. PD Fischer, et al., Hsthot-jupiter transmission spectral survey: Clear skies for cool saturn wasp-39b. *The Astrophys. J.* **827**, 19 (2016).
5. HA Knutson, et al., Aspitzertransmission spectrum for the exoplanet gj 436b, evidence for stellar variability, and constraints on dayside flux variations. *The Astrophys. J.* **735**, 27 (2011).
6. P Goudfrooij, L Albert, R Doyon, The single-object slitless spectroscopy mode of webb's niriss instrument (2015).
7. Jwst user documentation: Niriss (jwst_docs.stsci.edu) (2017).
8. IN Sokolik, Absorption by atmospheric gases in the ir, visible and uv spectral regions (EAS8803_Fall2009) (2009).
9. Niriss-soss planning tool (http://maestria.astro.umontreal.ca/niriss/SOSS_cont/SOSScontam.php) (2020).
10. MD Perrin, et al., Updated point spread function simulations for JWST with WebbPSF in *Space Telescopes and Instrumentation 2014: Optical, Infrared, and Millimeter Wave*, Society of Photo-Optical Instrumentation Engineers (SPIE) Conference Series, eds. J Oschmann, Jacobus M., M Clampin, GG Fazio, HA MacEwen. Vol. 9143, p. 91433X (2014).